Channeling of multikilojoule high-intensity laser beams in an inhomogeneous plasma

S. Ivancic, D. Haberberger, H. Habara, T. Iwawaki, K. S. Anderson, R. S. Craxton, D. H. Froula, D. D. Meyerhofer, C. Stoeckl, K. A. Tanaka, and W. Theobald

Phys. Rev. E **91**, 051101 — Published 4 May 2015

DOI: 10.1103/PhysRevE.91.051101

Channeling of Multi-kJ High-Intensity Laser Beams in an Inhomogeneous Plasma

S. Ivancic,[1,2,*] D. Haberberger,[1] H. Habara,[3] T. Iwawaki,[3] K. S. Anderson,[1] R. S. Craxton,[1]
D. H. Froula,[1,4] D. D. Meyerhofer,[1,2,4] C. Stoeckl,[1] K. A. Tanaka,[3] and W. Theobald[1]

[1]*Laboratory for Laser Energetics, University of Rochester, Rochester, New York 14623, USA*
[2]*Department of Mechanical Engineering, University of Rochester, Rochester, New York, 14623, USA*
[3]*Division of Electric, Electronic, and Information, Graduate School of Engineering, Osaka University, Osaka, Japan*
[4]*Department of Physics and Astronomy, University of Rochester, Rochester, New York, 14623, USA*

(Dated: April 21, 2015)

Channeling experiments were performed that demonstrate the transport of high-intensity ($>10^{18}$-W/cm^2), multikilojoule laser light through a millimeter-sized, inhomogeneous ($\sim$300-μm density scale length) laser-produced plasma up to overcritical density, which is an important step forward for the fast-ignition concept. The background plasma density and the density depression inside the channel were characterized with a novel optical probe system. The channel progression velocity was measured for the first time, which agrees well with theoretical predictions based on large scale particle-in-cell simulations, confirming scaling laws for the required channeling laser energy and laser pulse duration, which are important parameters for future integrated fast-ignition channeling experiments.

The propagation of a laser beam at relativistic intensities ($>10^{18}$ W/cm^2) through plasma with a large density scale length is dominated by highly nonlinear interactions including ponderomotive expulsion of electrons [1], channeling [2–4], and the development of hosing and bifurcation instabilities [3, 4]. These effects are important for both fundamental aspects of relativistic laser–plasma interaction physics and applications such as fast ignition in inertial confinement fusion [5]. The central idea of the fast-ignition concept is to first compress a frozen DT-ice capsule with a nanosecond, megajoule laser to a high areal density and then use an ultrapowerful short-pulse laser to subsequently ignite the fuel. Since laser light at nonrelativistic intensities propagates in the plasma corona up to only the critical density $n_c = \omega_0^2 m_e \varepsilon_0 / e^2$ (ω_0 is the laser angular frequency, m_e is the electron mass, ε_0 is the permittivity of free space, and e is the elementary charge), the idea is to use one high-intensity pulse to form a channel through the corona and then inject the ignition pulse into the lower-density plasma column as in an optical waveguide [6] to deposit sufficient energy in the core for ignition. In contrast to the cone-in-shell concept [7], the channeling concept has the advantage that it uses symmetric implosions and can be readily applied to cryogenic targets.

Channeling into dense plasmas relies on high laser intensity to provide sufficient ponderomotive pressure against the outflowing plasma and a long-enough laser pulse duration to sustain the channel formation. When the laser reaches densities $> n_c$, it may continue to push forward through its ponderomotive pressure ("hole-boring") and relativistic transparency. The ponderomotive hole-boring velocity [8, 9] is found by balancing the light pressure against the pressure arising from the material stagnating against the head of the channel. For an increasing laser intensity, a higher hole-boring velocity is obtained.

Channeling experiments with short [10] and long [11] laser pulses were performed, and it was demonstrated both in experiments [12] and simulations [4] that channels have a higher transmission for a trailing pulse compared to unperturbed plasma. These experimental observations were carried out using a variety of diagnostics including interferometry [12], self-emission [13], and x-ray grid image refractometry [14]. The effect of the radiation pressure on plasma at the critical density surface has been already observed in experiments with 1-μm wavelength, low intensity ($\sim 3\times10^{14}$ W/cm^2) laser radiation interacting with very short-density-scale-length ($\sim 1-\mu$m) plasmas [15] well before the fast-ignition concept was proposed. These experiments applied a 15-ps, 0.266-μm probe laser and interferometry to measure plasma densities up to $\sim$1.7 n_c of the IR beam. However, the short scale length and the low intensity render these experiments irrelevant for fast ignition, which requires the study of plasmas with density scale lengths of several hundred μm and relativistic laser intensities. Later experiments [14] claimed the observation of the propagation of a short-pulse, high-intensity laser beyond n_c in inhomogeneous plasma with scale length of $\sim$100 μm. However, the x-ray laser grid image refractometry technique [14] suffered from a poor imaging quality, which makes it difficult to identify the channel. Higher-quality data were obtained in our work that clearly shows the channel formation.

This communication describes the first observation of laser channeling in millimeter-sized inhomogeneous plasma to overcritical densities with high energy ($\sim$kJ), short (10-ps and 100-ps) infrared (IR) laser pulses with peak intensities between $\sim 1\times10^{19}$ and $\sim 4\times10^{19}$ W/cm^2. This experimental study is the first of its kind with fast-ignition–relevant parameters including sufficiently long density scale length at n_c comparable to high-compression OMEGA laser implosions, relativistic laser intensities, $\sim$kJ laser energies, and the application of a novel high-quality optical probing technique that characterizes densities $>n_c$ of the IR light. Measurements of the plasma density in the channel and in the background plasma are presented. This singularizes our experiment as the one that is currently the most relevant for the fast-ignition channeling concept and provides important guiding for future integrated fast-ignition channeling experiments. In addition, a comparison of the channeling performance for two different

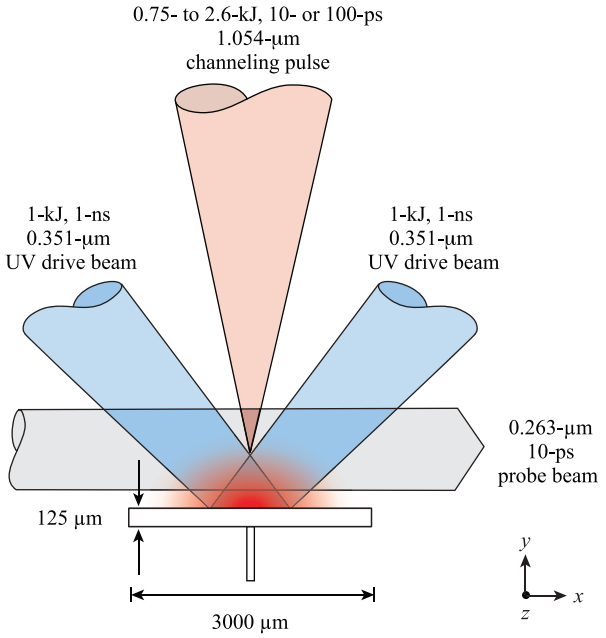

FIG. 1. (Color online) Schematic of the experimental setup. A plastic target is illuminated by two UV drive beams to generate a large expanding plasma plume. Following the UV drive beams, an IR channeling laser beam is injected into the plume along the density gradient. The interaction is observed by an UV optical probe pulse that is timed to arrive at a specific delay from the start of the channeling pulse.

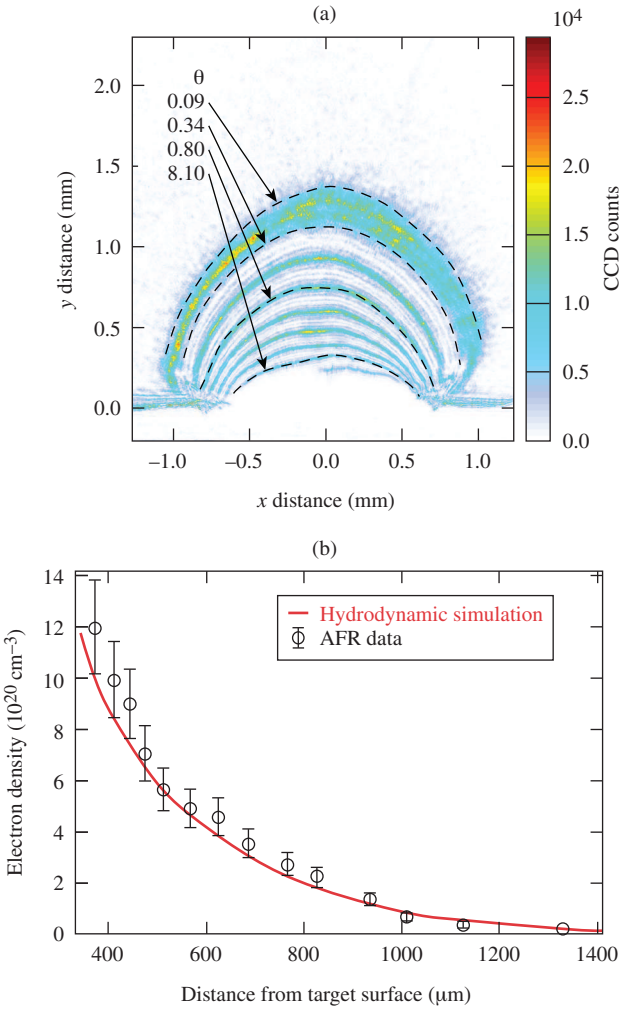

FIG. 2. (Color online) (a) Measured optical probe image of the unperturbed long-scale-length plasma (45 ps prior to the arrival of the channeling beam). The original target surface is located at $y = 0$. Contours of constant refraction angle and the associated electron densities are also shown. (b) On-axis lineout of the measured values of the unperturbed electron density (points) versus distance from the target surface. The solid line is a prediction from a 2-D hydrodynamics simulation.

laser pulse durations (10 and 100 ps) is presented, which sheds light on the scaling laws of the required laser energy and the progression time of the channel front from the laser focus to n_c. From the comparison of our experimental results to large scale particle-in-cell (PIC) simulations we identified the main physical interaction mechanisms as the ponderomotive expulsion of plasma material and the density pile-up in front of the channel head, which causes the slowing down of the channel progression when the critical density is approached. To the best of our knowledge, this presents the first experimental demonstration of the slowing down of the channel propagation in overdense inhomogeneous plasma.

The experiments were carried out on the OMEGA EP Laser System [16]. Figure 1 shows a schematic of the interaction and probing geometries. Two ultraviolet (UV) ($\lambda_{UV} = 0.351$ μm) laser beams (f = 6.5) smoothed by distributed phase plates (eighth-order super-Gaussian with 800-μm full width at half maximum) [17] irradiated a 125-μm-thick planar plastic (CH) target to create and heat a blowoff plasma. The UV irradiation delivered 2 kJ of total energy in a 1-ns square pulse. The channeling laser pulse was an IR ($\lambda_{IR} = 1.054$-μm) beam with an energy ranging from 0.75 kJ to 2.6 kJ. An intensity comparison was performed by using 100-ps and 10-ps pulse widths, respectively. The wavefront of the channeling beam was measured and the focal-spot irradiance map was inferred for each shot [18]. The vacuum focal spot contained 80% of the laser energy in a 20-μm-radius spot with peak intensities of $\sim 1 \times 10^{19}$ and $\sim 4 \times 10^{19}$ W/cm^2 for 2.6-kJ, 100-ps and 1-kJ, 10-ps pulses, respectively. The average laser intensities in the focal spot are about an order of magnitude lower. The focal position of the channeling beam was set to 750 μm from the original target surface, and the corresponding electron plasma density was predicted to be $n_e = 2.5 \times 10^{20}$ cm^{-3}, which is close to $n_c/4$. It has been suggested in Ref. [19] that focusing the laser beam to $n_c/4$ might provide the most-favorable condition for relativistically enhanced propagation. The probe beam [20] was a 10-ps, 0.263-μm laser with 10 mJ of energy. The relative timing between the probe and channeling pulse was measured with an accuracy of better than 20 ps on each shot.

The observations reported here were made possible by em-

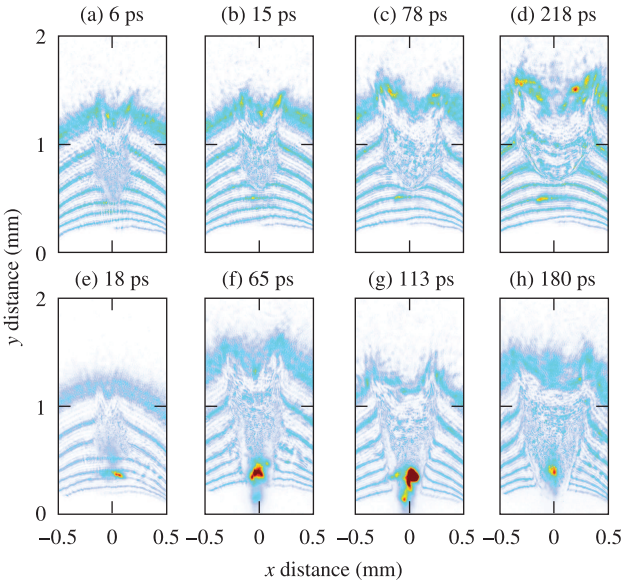

FIG. 3. (Color online) Optical probe images for 10-ps and 100-ps channeling laser pulses at various times showing greater penetration depth for the longer pulse. The red spots in (e)-(h) are caused by fourth-harmonic generation from the 100-ps, 20-TW channeling pulse reaching n_c. The 10-ps, 125-TW laser pulse [(a)-(d)] never reaches n_c and therefore does not produce fourth-harmonic emission. Since the detector integrated over a time much longer than the duration of the probe pulse, the harmonic signal is present even in frames taken before the channel reaches the critical surface in the probe image. Time zero is defined as the start of the short pulse. The background plasma was always the same as the one shown in Fig. 2(a).

ploying a short probe wavelength and a sufficiently large solid angle of the collection optics ($f \approx 4$). The expanding blowoff plasma was measured by using a new method of optical probing, angular filter refractometry (AFR) [21], which visualizes gradients in the refractive index n of an unmagnetized, collisionless plasma, given by $n = \sqrt{1 - n_e/n_c}$. Figure 2(a) shows an example of such a measurement shortly before the arrival of the channeling beam. The probe light that has passed through the plasma is collected and filtered in the focal plane of the collection optics where the spatial location of probing rays depend on their refraction angle. A bullseye-patterned filter with alternating transparent and opaque rings provides isocontours of the refraction angle in the image plane. Using AFR allows one to measure the angular deviation of probe rays while preserving the fine structures in the image, which is a considerable advantage over other methods. AFR, as a refractive method, is capable of probing large plasma volumes, whereas, e.g., interferometric techniques that rely on fringe-shift measurements are severely limited by the large phase shifts accumulated along the path [22]. The reason why interferometry, which was used in Ref. [12] and [13] as the primary probing technique, cannot be applied in our experiment is simply because of the large size and the high density of the plasma. As the UV probe passes through the high-density regions of the plasma, the interference fringes become closer until they are unresolvable. The accumulated phase is greater than 1000 rad resulting in more than 160 fringe shifts over a distance of ∼1 mm, therefore giving one fringe shift over ∼6 μm, which is very close to the instrumental resolution (4 μm). The electron plasma density profile shown in Fig. 2(b) was inferred from the measured angular deviation θ of probing rays assuming a hemispherical plasma with a varying refractive index. The analysis is described in detail in Ref. [21]. The unperturbed on-axis plasma profile in Fig. 2(b) is in agreement with two-dimensional (2-D) hydrodynamic simulations with the code *DRACO* [23]. The simulated electron temperature is 1.8 keV. The experimentally determined radial density scale length in the observed region varies from 200 to 320 μm with 250 μm being the average. The last contour in the collection system ($\theta \approx 8.1^\circ$) corresponds to light that is refracted through a peak density above n_c (1.4×10^{21} cm^{-3}). Strong refractive index gradients in the plasma might affect the data analysis if the curvatures of the ray paths are not taken into account. Electron density reconstruction based on inversion procedures that assume straight paths tend to underestimate the density in the dense plasma part [24]. The error is small (less than 12%) for our conditions and therefore the straight path assumption is a good approximation. This was estimated based on calculations with an optical ray-trace code that properly takes the refraction in an artificial plasma object into account and caluclating a synthetic AFR image that was then analysed assuming straight optical paths [21]. Together with an error of 3% in the absolute calibration of the refraction angles, the total error is calculated to be 15%.

Figure 3 shows measured channels at different probing times for 10-ps and 100-ps laser irradiation. The short pulses were injected in the plasma 1-ns after the start of the UV-pulse. The channel is visualized by the perturbations in the AFR contours. The contours bend as a result of strong density gradients created by the channeling pulse. The top row in Fig. 3 shows the results for the 10-ps pulse. The head of the channel reached at 6 ps to a position 450 μm from the original target surface, corresponding to 0.6 n_c. Time zero corresponds to when the pulse arrives at the normal focus position 750 μm away afrom the target. The channel was observed up to 200 ps after its creation. Later in time, the tip of the channel retreats backward with a velocity of $\sim 3\times10^7$cm/s away from the target surface. There is a clear difference in the channel depth between the 10-ps and 100-ps pulses. The 100-ps pulse (bottom row) reaches to the contour closest to the original target surface, indicating that a density $> 1.4\times10^{21}$cm^{-3} has been reached. The 100-ps pulse shown in Fig. 3(e) reached in only 18 ps to about the same depth as the 10-ps pulse. The 100-ps pulse continued to bore through the plasma, reaching overcritical density at 65 ps after the start of the laser beam. The upper contour bands in the lower-density region are smoothly shifted in space, while the contours at higher density inside the channel are highly distorted and obscured. This is likely caused by sharp density modulations at the channel wall that are also observed in PIC simulations [3, 25]. Bright fourth-

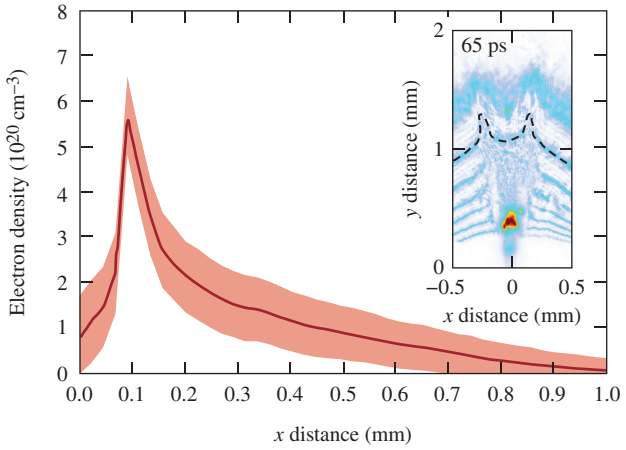

FIG. 4. (Color Online) Density profile of a channel created by a 100-ps pulse and probed at ∼65 ps into the pulse along the x axis at $y = 0.8$ mm. The density on axis is reduced by ∼60% with respect to the density of the unperturbed plasma at the same location ($n_e = 2\times10^{20}$ cm^{-3}). Error bars are calculated from the uncertainty in the measurement of θ.

harmonic emission of the channeling beam was measured in the vicinity of the critical surface [Figs. 3(e)-3(h)] with the 100-ps pulse. Harmonics from the critical-density surface have been observed in experiments with high-intensity laser beams interacting with solid-density plasmas [26]. No harmonic emission was observed with the 10-ps pulse, confirming that it did not reach n_c.

Figure 4 shows a radial cross section of the measured density profile in the channel. The density is calculated using an Abel inversion of the phase, which is inferred from the angular refraction in the AFR image. The density profile in the channel region takes on a parabolic-like shape bounded on either side by walls with a density higher than the background density. For the specific image shown here, the density in the channel has been reduced from 2×10^{20} cm^{-3} to 8×10^{19} cm^{-3}—a reduction of 60%. This image was taken at 65 ps into a 100-ps pulse, so the density may be reduced further. At later times, contours become impossible to identify as the density gradient at the channel wall steepens.

The intensity distribution in the experimental laser focus was not diffraction limited and contained some spatial inhomogeneity [18], which probably seeded the filamentation instability and self-focusing in the plasma driven by ponderomotive and relativistic effects. Filamentation was predicted by a split-step paraxial wave equation calculation taking the ponderomotive and relativistic effects into account and using the measured wavefront map of the channeling beam and the refractive index of the plasma. In addition, simultaneous measurements of the strong electrostatic and magnetic fields inside the plasma with proton radiography [27] also concluded the existence of filamentated structures at a location between 0.5 and 1 mm from the initial target surface. Three-dimensional (3-D) hydrodynamic simulations including relativistic corrections and the effect of charge separation have demonstrated that aberrated beams do not channel as effectively as diffraction-limited beams [28]. Filamentation is sensitive to the power in the laser speckles and therefore is expected to be more severe for higher-power pulses. When sufficiently driven, this might cause beam spraying and result in the breakup of the beam so that it cannot reach a higher density. The 100-ps channeling beam had $\sim 4\times$ less power than the 10-ps pulse and is expected to be less affected by filamentation, which might be one of the reasons why this beam propagated deeper into the plasma.

Two- and three-dimensional PIC simulations with large (∼500-μm) plasmas studied the propagation and channeling for conditions similar to the experiment in a plasma density profile of the shape $n_e = 0.1 n_c \exp(x/L)$ with $L = 430$ μm [3, 4]. The laser power greatly exceeds the power threshold for relativistic self-focusing [29, 30] and beam filamentation occurs in the early stage of the simulation. The local intensity increases in the filaments and the resulting transverse ponderomotive force pushes most of the electrons out of the filaments. The resulting space-charge force causes the ions to follow, creating several microchannels that eventually merge together and form a single density channel along the laser propagation axis. The simulations predict that besides laser hosing, channel bifurcation, and self-correction, the laser front will pile up material at the channel head that will reach densities $> n_c$, even though the surrounding plasma is underdense. The simulations predict that after a short initial period (∼ps), when the pulse propagates with a speed close to the linear group velocity, it quickly slows down and, after ∼5 ps, approaches the ponderomotive hole-boring velocity [8, 9]. The plasma density gradient rapidly steepens in front of the pulse and the laser light essentially interacts most of the time with steep overcritical plasma [3, 4].

The channel progression velocity can be obtained from the experiment. The depth of the channel is found by measuring the distance from the original target surface to the closest point of perturbed contours in the probe image. For early times [Fig. 3(a) and 3(b)] during the laser interaction, the progression velocity is between ∼50 and ∼20 μm/ps, but at later times (65 ps) during the 100-ps pulse interaction, when the laser propagated deeper into the plasma, the channel progression velocity slows down to ∼3 μm/ps. The Mach angle gives another measure of the velocity of the supersonic advancing front in the gas. The velocity of the front of the channel is found by measuring the angle of the wake left behind by the channel. The Mach angle relates the front Mach number M to the angle θ_m by $\sin(\theta_m) = 1/M$. At 65 ps the Mach angle is measured to be ∼8° [in Fig. 3(f)], which gives a Mach number of ∼7 and a velocity of 2 μm/ps, slightly lower than from the depth measurement.

The measured channel progression velocity is in agreement with PIC simulations showing that it approaches the hole-boring velocity, given by $v_h = c\sqrt{Z(n_c/n_e)(m_e/M_i)(2-\eta_a)I_{18}\lambda_\mu^2/5.48}$ for normal incidence light [9]. Here c is the speed of light, Z the

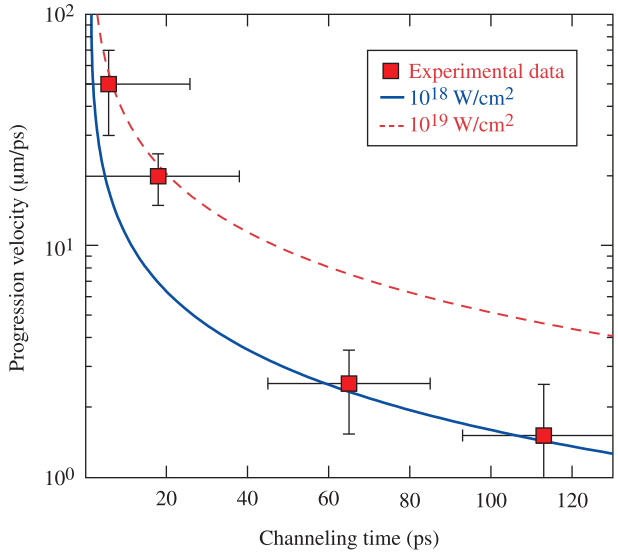

FIG. 5. (Color online) Measured channel progression velocity (squares) as a function of channeling time through the plasma. The solid and dashed curves are from a 2-D particle-in-cell simulation [3].

average charge state of the plasma, M_i the ion mass, η_a the laser energy absorption fraction, I_{18} the laser intensity in units of $10^{18} W/\mathrm{cm}^2$, and λ_μ the laser wavelength in units of μm. The hole-boring velocity decreases with $1/\sqrt{n_e}$ when the pulse propagates deeper into the plasma, forcing more material to pile up. The simulations [3] show for propagation through a background density of $\sim 0.2 n_c$ that the pile up is moderate and reaches $\sim 0.3 n_c$ (an increase of $\sim$30%), while for a background density of $\sim 0.5 n_c$ the density is doubled to $\sim 1 n_c$. For an average intensity of $I = 10^{18}$ W/cm^2, fully ionized plastic, η_a=1, and n_e/n_c = 1 v_h is estimated with 2.2 μm/ps, respectively, which is consistent with the measurement. When propagating through the underdense range with no significant pile-up, the progression speed is close to the group velocity. For a background density of, e.g., $n_e/n_c = 0.3$ the progression speed approaches according to simulations [3] $\sim$60 μm/ps, a value between the local group velocity and the hole-boring velocity. Figure 5 shows the measured progression velocity as a function of the channeling time and compares it with the velocity inferred from a 2-D simulation at laser intensities of 1×10^{18} and 1×10^{19} W/cm^2.

The 3-D simulations [4] provide scalings for the time T_c that is required for the channel head to reach the position of n_c and the required laser energy E_c, which are given by $T_c(\mathrm{ps}) = 1.5 \times 10^2 (L_\mu/430) I_{18}^{-0.64}$ and $E_c(\mathrm{kJ}) = 0.85 (L_\mu/430) I_{18}^{0.32}$, where L_μ is the density scale length in μm. The estimated times and energies are between $\sim$20 ps, 1.1 kJ and $\sim$90 ps, 0.5 kJ for 10^{19} W/cm^2 and 10^{18} W/cm^2, respectively, in rough agreement with the experimental values. This scaling also demonstrates that the 10-ps pulse is too short to reach n_c.

In conclusion, channeling experiments were performed under fast-ignition–relevant conditions ($\sim$300-μm density scale length, channeling pulse energies >1 kJ, and relativistic intensity) in a large inhomogeneous plasma to overcritical densities. The experiments show that 100-ps infrared pulses with a peak intensity of $\sim 1 \times 10^{19}$ W/cm^2 evacuate a cavity to plasma densities beyond critical. The cavity in the plasma forms in less than 100 ps, and advances in dense background plasma at a velocity of ~ 2 μm/ps.

This work was supported by the U.S. Department of Energy National Nuclear Security Administration under Award Number DE-NA0001944, the OFES ACE Fast Ignition grant No. DE-DE-FG02-05ER54839, the DOE Laboratory Basic Science Program, the University of Rochester, and the New York State Energy Research and Development Authority. The support of DOE does not constitute an endorsement by DOE of the views expressed in this Letter. We acknowledge the support with PIC simulations by G. Li and C. Ren. Part of this work is supported with the Grant-in-Aid for Scientific research A (No. 22246122) and B (No. 23360412) as well as with the Japan-U.S. Collaboration in Fusion Research and Development under MEXT and NIFS.

* siva@lle.rochester.edu

[1] K.-C. Tzeng and W. B. Mori, Phys. Rev. Lett. **81**, 104 (1998).
[2] A. Pukhov and J. Meyer-ter Vehn, Phys. Rev. Lett. **76**, 3975 (1996).
[3] G. Li, R. Yan, C. Ren, T.-L. Wang, J. Tonge, and W. B. Mori, Phys. Rev. Lett. **100**, 125002 (2008).
[4] G. Li, R. Yan, C. Ren, J. Tonge, and W. B. Mori, Physics of Plasmas (1994-present) **18**, 042703 (2011).
[5] M. Tabak, J. Hammer, M. E. Glinsky, W. L. Kruer, S. C. Wilks, J. Woodworth, E. M. Campbell, M. D. Perry, and R. J. Mason, Phys. Plasmas **1**, 1626 (1994).
[6] C. G. Durfee and H. M. Milchberg, Phys. Rev. Lett. **71**, 2409 (1993).
[7] R. Kodama, P. A. Norreys, K. Mima, A. E. Dangor, R. G. Evans, H. Fujita, Y. Kitagawa, K. Krushelnick, T. Miyakoshi, N. Miyanaga, T. Norimatsu, S. J. Rose, T. Shozaki, K. Shigemori, A. Sunahara, M. Tampo, K. A. Tanaka, Y. Toyama, T. Yamanaka, and M. Zepf, Nature **412**, 798 (2001).
[8] W. L. Kruer, E. J. Valeo, and K. G. Estabrook, Phys. Rev. Lett. **35**, 1076 (1975).
[9] S. C. Wilks, W. L. Kruer, M. Tabak, and A. B. Langdon, Phys. Rev. Lett. **69**, 1383 (1992).
[10] K. A. Tanaka, R. Kodama, Y. Kitagawa, K. Kondo, K. Mima, H. Azechi, Z. Chen, S. Fujioka, H. Fujita, T. Johzaki, A. Lei, T. Matsuoka, K. Mima, N. Miyanaga, K. Nagai, H. Nagatomo, H. Nishimura, T. Norimatsu, K. Shigemori, H. Shiraga, M. Tanpo, Y. Tohyama, T. Yabuuchi, J. Zheng, Y. Izawa, P. A. Norreys, R. Stephens, and S. Hatchett, Plasma Physics and Controlled Fusion **46**, B41 (2004).
[11] P. E. Young, M. E. Foord, J. H. Hammer, W. L. Kruer, M. Tabak, and S. C. Wilks, Phys. Rev. Lett. **75**, 1082 (1995).
[12] J. Fuchs, E. d'Humières, Y. Sentoku, P. Antici, S. Atzeni, H. Bandulet, S. Depierreux, C. Labaune, and A. Schiavi, Phys. Rev. Lett. **105**, 225001 (2010).
[13] M. Borghesi, A. J. MacKinnon, L. Barringer, R. Gaillard, L. A. Gizzi, C. Meyer, O. Willi, A. Pukhov, and J. Meyer-ter Vehn, Physical Review Letters **78**, 879 (1997).

[14] K. Takahashi, R. Kodama, K. A. Tanaka, H. Hashimoto, Y. Kato, K. Mima, F. A. Weber, T. W. Barbee, and L. B. Da Silva, Phys. Rev. Lett. **84**, 2405 (2000).

[15] D. T. Attwood, D. W. Sweeney, J. M. Auerbach, and P. H. Y. Lee, Phys. Rev. Lett. **40**, 184 (1978).

[16] L. Waxer, D. Maywar, J. Kelly, T. Kessler, B. Kruschwitz, S. Loucks, R. McCrory, D. Meyerhofer, S. Morse, C. Stoeckl, and J. Zuegel, Optics Photonics News **16**, 30 (2005).

[17] H. Powell and T. Kessler, *Laser Coherence Control: Technology and Applications : 21-22 January 1993, Los Angeles, California*, Proceedings of SPIE–the International Society for Optical Engineering No. v. 1870 (SPIE–the International Society for Optical Engineering, 1993).

[18] B. E. Kruschwitz, S.-W. Bahk, J. Bromage, M. D. Moore, and D. Irwin, Opt. Express **20**, 20874 (2012).

[19] T. Matsuoka, A. Lei, T. Yabuuchi, K. Adumi, J. Zheng, R. Kodama, K. Sawai, K. Suzuki, Y. Kitagawa, T. Norimatsu, K. Nagai, H. Nagatomo, Y. Izawa, K. Mima, Y. Sentoku, and K. A. Tanaka, Plasma Physics and Controlled Fusion **50**, 105011 (2008).

[20] D. H. Froula, R. Boni, M. Bedzyk, R. S. Craxton, F. Ehrne, S. Ivancic, R. Jungquist, M. J. Shoup, W. Theobald, D. Weiner, N. L. Kugland, and M. C. Rushford, Review of Scientific Instruments **83**, 10E523 (2012).

[21] D. Haberberger, S. Ivancic, S. X. Hu, R. Boni, M. Barczys, R. S. Craxton, and D. H. Froula, Phys. Plasmas **21**, 056304 (2014).

[22] R. S. Craxton, F. S. Turner, R. Hoefen, C. Darrow, E. F. Gabl, and G. E. Busch, Physics of Fluids B: Plasma Physics **5**, 4419 (1993).

[23] P. B. Radha, T. J. B. Collins, J. A. Delettrez, Y. Elbaz, R. Epstein, V. Y. Glebov, V. N. Goncharov, R. L. Keck, J. P. Knauer, J. A. Marozas, F. J. Marshall, R. L. McCrory, P. W. McKenty, D. D. Meyerhofer, S. P. Regan, T. C. Sangster, W. Seka, D. Shvarts, S. Skupsky, Y. Srebro, and C. Stoeckl, Physics of Plasmas **12**, 056307 (2005).

[24] D. W. Sweeney, D. T. Attwood, and L. W. Coleman, Appl. Opt. **15**, 1126 (1976).

[25] L. Willingale, P. M. Nilson, A. G. R. Thomas, J. Cobble, R. S. Craxton, A. Maksimchuk, P. A. Norreys, T. C. Sangster, R. H. H. Scott, C. Stoeckl, C. Zulick, and K. Krushelnick, Phys. Rev. Lett. **106**, 105002 (2011).

[26] J. Zhang, M. Zepf, P. A. Norreys, A. E. Dangor, M. Bakarezos, C. N. Danson, A. Dyson, A. P. Fews, P. Gibbon, M. H. Key, P. Lee, P. Loukakos, S. Moustaizis, D. Neely, F. N. Walsh, and J. S. Wark, Phys. Rev. A **54**, 1597 (1996).

[27] Y. Uematsu, S. Ivancic, T. Iwawaki, H. Habara, A. L. Lei, W. Theobald, and K. A. Tanaka, Review of Scientific Instruments **85**, 11E612 (2014).

[28] D. E. Hinkel, E. A. Williams, R. L. Berger, L. V. Powers, A. B. Langdon, and C. H. Still, Physics of Plasmas **5**, 1887 (1998).

[29] C. E. Max, J. Arons, and A. B. Langdon, Phys. Rev. Lett. **33**, 209 (1974).

[30] B. I. Cohen and C. E. Max, Physics of Fluids **22**, 1115 (1979).